Chinese Chemical Letters 35 (2024) 109146

Contents lists available at ScienceDirect

Chinese Chemical Letters

journal homepage: www.elsevier.com/locate/cclet

A weakly-solvated ether-based electrolyte for fast-charging graphite anode

Xiao Zhu, Yanbing Mo, Jiawei Chen, Gaopan Liu, Yonggang Wang, Xiaoli Dong*

Department of Chemistry and Shanghai Key Laboratory of Molecular Catalysis and Innovative Materials, Institute of New Energy, iChEM (Collaborative Innovation Center of Chemistry for Energy Materials), Fudan University, Shanghai 200433, China

ARTICLE INFO

Article history:
Received 11 August 2023
Revised 6 September 2023
Accepted 22 September 2023
Available online 28 September 2023

Keywords:
Weakly-solvated solvent
Bisalt ether-based electrolyte
Graphite anode
NCM||graphite battery
Interfacial optimization

ABSTRACT

Weakly-solvated electrolytes (WSEs) utilizing solvents with weak coordination ability offer advantages for low-potential graphite anode owing to their facile desolvation process and anions-derived inorganic-rich solid electrolyte interphase (SEI) film. However, these electrolytes face challenges in achieving a balance between the weak solvation affinity and high ionic conductivity, as well as between rigid inorganic-rich SEI and flexible SEI for long-term stability. Herein, we introduce 1,3-dioxolane (DOL) and lithium bis(trifluoromethanesulfonyl)-imide (LiTFSI) as functional additives into a WSE based on nonpolar cyclic ether (1,4-dioxane). The well-formulated WSE not only preserves the weakly solvated features and anion-dominated solvation sheath, but also utilizes DOL to contribute organic species for stabilizing the SEI layer. Benefitting from these merits, the optimized electrolyte enables graphite anode with excellent fast-charging performance (210 mAh/g at 5 C) and outstanding cycling stability (600 cycles with a capacity retention of 82.0% at room temperature and 400 cycles with a capacity retention of 80.4% at high temperature). Furthermore, the fabricated $LiNi_{0.8}Co_{0.1}Mn_{0.1}O_2$||graphite full cells demonstrate stable operation for 140 cycles with high capacity retention of 80.3%. This work highlights the potential of tailoring solvation sheath and interphase properties in WSEs for advanced electrolyte design in graphite-based lithium-ion batteries.

Throughout the history of lithium-ion batteries (LIBs), the success of graphite (Gr) anode, with its reversible Li^+ intercalation chemistry occurring at a low potential (~0.2 V *vs.* Li/Li^+), underscores the significance of the electrolyte and the corresponding Gr/electrolyte interphase [1,2]. The electrolyte plays a pivotal role in LIBs by facilitating ionic current conduction while insulating the electron flow between the two electrodes [3–5]. The ionic conductivity relies on the dissociation of lithium salt in polar solvents, wherein Li^+ become solvated with solvent molecules and exist in the form of solvated Li^+ ions. The extent of binding affinity between Li^+ and solvent molecules directly influences salt dissociation and ionic conductivity in the liquid electrolyte. A stronger binding energy results in more salt dissociation and higher ionic conductivity [6,7]. However, the strong affinity between Li^+-solvent leads to difficulties in the de-solvation process at the electrode/electrolyte interface, causing increased polarization and reduced capacity of Gr anode, particularly under high rates [8]. Consequently, it poses a challenge on electrolytes to strike a balance between achieving high ionic conductivity and promoting weakly solvated Li^+ ions.

Besides the role as ion conductor of electrolyte, it is generally considered that the primary Li^+-solvation sheath of the electrolyte is the main origin of the solid electrolyte interphase (SEI) layer, which plays a prominent role in determining the charge transfer kinetics across the interphase [9–11]. The decomposition of electrolyte components produces solid products including inorganic and organic species. The former often originates from the decomposition of inorganic Li salts, where the rigid inorganic ingredients such as Li_2CO_3 and Li_2O can provide smooth Li^+ conductivity across the SEI film. The latter arises from the initial decomposition of organic solvents, and these soft organic products contribute to the formation of an adhesive film on the electrode, ensuring long-term stability of electrode materials [12–14]. In general, an inorganic-rich SEI is preferred to optimize Li^+ migration and reduce polarization for the low-potential Gr anode. Encouraged by this, numerous strategies for electrolyte modification have been proposed, including high concentration electrolytes (HCE) [15,16], localized high concentration electrolytes (LHCE) [17–19], fluorinated solvents [20–22] and so forth. However, these electrolytes have limitations such as high cost from the salt or environmental

* Corresponding author.
E-mail address: xldong@fudan.edu.cn (X. Dong).

https://doi.org/10.1016/j.cclet.2023.109146
1001-8417/

risks from fluorine-containing species, resulting in a compromise between electrochemical performance and large-scale applications.

Recently, weakly-solvated electrolytes (WSEs) have been promoted as promising alternative for LIBs [23–25], which utilize solvents with weak solvation ability to weaken the interaction between Li^+ and solvent. This allows more anions to participate in the solvation sheath, forming contact ion pairs (CIPs) and aggregates (AGGs) resembling that in HCE or LHCE. As a result, an inorganic-rich anion-derived SEI is formed, which facilitates Li^+ transport across the SEI and promotes interface dynamics [26]. Commonly-used WSE solvents, such as 1,3-dioxolane (DOL), 1,4-dioxane (DX) and tetrahydrofuran (THF), are representative cyclic ethers with low dielectric constants (ε), exhibiting advantages in the de-solvation process for weakened Li^+-solvent interaction [27,28]. However, a notable drawback of WSEs is their weak solvent-ion interaction, leading to insufficient ionic conductivity due to the limited dissociation ability of Li^+ from its counter-anion. Furthermore, although the inorganic-rich SEI is conducive to fast ion transport, organic components like ROLi and $ROCO_2Li$ are essential for accommodating volume expansion during cycling to maintain the battery system's stability [27]. Consequently, using WSE solvents exclusively for LIBs results in poor cycling capability due to the absence of organic species in the SEI [24]. Therefore, it remains challenging for WSEs to realize the trade-off between the rigid inorganic SEI components for facile desolvation and charge transfer at the interface and flexible organic SEI compositions for repeated (de)-intercalation and stable cycling, along with achieving high ionic conductivity.

Herein, a weakly-solvated bisalt ether-based electrolyte (LTDD) was delicately formulated based on a representative nonpolar cyclic ether DX by introducing DOL and lithium bis(trifluoromethanesulfonyl)imide (LiTFSI) as functional additives. These two additives not only facilitate the retention of high CIPs and AGGs contents in the DX-based electrolyte for the generation of inorganic-rich SEI, but also allow DOL to participate in the solvation structure to compensate organic components in SEI film. These advantages result in a high Li^+ transference number (t_{Li^+}) of 0.77, enabling the Gr anode with excellent rate performance (210 mAh/g at 5 C) and outstanding cycling stability for 600 cycles (82.0% capacity retention). Furthermore, Gr anodes maintain exceptional cycling stability for over 400 cycles at a high temperature of 50 °C. As for $LiNi_{0.8}Co_{0.1}Mn_{0.1}O_2$ (NCM811) cathode, LTDD displays impressive rate capability (140 mAh/g at 3 C). The NCM811||Gr full cell with LTDD delivers a high reversible capacity of 170 mAh/g at 1 C and maintains stable cycle for 140 cycles with remarkable capacity retention of 80.3%. These results highlight the significance of functional electrolyte components for excellent performance, expanding the potential applications of WSE in Gr anodes and Gr-based LIBs.

The DX molecule is a typical nonpolar cyclic ether with low permittivity and weak solvating ability. This can be proved with the relatively uniform charge distribution shown in the electrostatic potential (ESP) maps (Fig. 1a). Moreover, the negative charges are primarily localized on the O atoms, exhibiting the potential binding sites with Li^+. Similar to the cyclic DX, DOL is also a weakly-solvated solvent while exhibits slightly higher negativity on the O atoms. This can be further demonstrated with the binding energy calculated by density functional theory (DFT) (Fig. 1b). As it turns out, both DX and DOL have low binding energies with Li^+, promising the rapid desolvation process of Li^+. Moreover, the affinity of Li^+-DOL (−1.84 eV) is as expected stronger than that of Li^+-DX (−1.74 eV), in consistence with the ESP analysis. In addition, DOL was frequently employed in the construction of polymer electrolytes due to its facile ring-opening polymerization under FSI^- induction [29,30]. Therefore, DOL can be expected to act as an organic film-forming addictive in WSEs. The weak solvating ability of DX and DOL would lead to the difficulty in dissociating Li^+ from its counterpart anions, where lithium salts with large anions are preferred and LiFSI was herein chosen as the main salt due to its easy dissociation for sufficient ionic conductivity. In addition, it should be noted that the slightly stronger coordination ability of DOL with Li^+ than DX compromises the weakly-solvated characteristic to a certain extent, sacrificing the certain CIPs and AGGs in the WSE. Therefore, the bis(trifluoromethanesulfonyl)imide ($TFSI^-$) anions are further introduced owing to its strongest coordination ability with Li^+ (−6.13 eV) compared to FSI^- (−6.02 eV) and DOL (−1.84 eV), for the compensation of anion-domain solvation sheath. Based on this selection, a single-salt-single-solvent WSE electrolyte (1.0 mol/kg LiFSI in DX, referred to as LD) is prepared as the control electrolyte. Two other WSE electrolytes, one with DOL (1.0 mol/kg LiFSI in the mixture of DX and DOL, named as LDD), the other with DOL and bisalt (0.75 mol/kg LiFSI and 0.25 mol/kg LiTFSI in the mixture of DX and DOL, named as LTDD) are well formulated to prove the conjecture about the electrolyte components and their functions.

Prior to the detailed investigations of the three electrolytes (LD, LDD, LTDD), the weight ratio of DOL was firstly optimized and set as 20% in LDD and LTDD according to the ionic conductivity (σ), t_{Li^+} and their compatibility with Gr anode (Figs. S1 and S2 in Supporting information). It can be detected from Fig. 1c that LD electrolyte displays a low ionic conductivity of 1.92 mS/cm due to the limited solubility of DX, which results in incomplete dissociation of LiFSI and a small quantity of free ions. The introduction of DOL can improve the ionic conductivity owing to its slightly stronger coordination ability, which promotes the dissociation of lithium salts, as demonstrated with 2.70 mS/cm for LDD and 2.26 mS/cm for LTDD. Noteworthily, these electrolytes demonstrated notably high t_{Li^+} values (0.74 for LD, 0.73 for LDD and 0.77 for LTDD), which are much higher than that of commonly-used carbonate electrolyte LB010 (1.0 mol/L $LiPF_6$ in dimethyl carbonate (DMC):ethylene carbonate (EC):ethyl methyl carbonate (EMC) = 1:1:1 wt%, Fig. S3 in Supporting information). Such high t_{Li^+} values are advantageous for Li^+ movement by mitigating the concentration polarization and offsetting the deficiency of low ionic conductivity, thereby facilitating fast Li^+ kinetics in the electrolytes [31,32].

Raman spectroscopy was further utilized to gain deep insight into the solvation structures of these electrolytes (Fig. S4 in Supporting information). Compared with the pure DX solvent, the Raman shift located at 1017 cm^{-1} corresponding to O–C-C stretching slightly shifted to a higher Raman shift in the investigated electrolytes, attributing to the extremely weak coordination of Li^+ with DX, which is consistent with above-mentioned weakly-solvated characteristic of DX (Fig. 1d). Similar findings can also be detected at 425 cm^{-1} corresponding to C–O-C bending, 437 cm^{-1} corresponding to C–C-O bending and 837 cm^{-1} corresponding to C–O-C stretching (Fig. 1d and Fig. S5 in Supporting information) [33]. The solvation behavior can be clearly detected with Raman shift of anions, as illustrated in Fig. 1e. The S-N-S bending signal FSI^- and $TFSI^-$ can be classified into four distinctive bands: free FSI^- anions (719 cm^{-1}, non-coordinated FSI^-), CIPs for FSI^- (733 cm^{-1}, one FSI^- binding with one Li^+), combining CIPs for $TFSI^-$ and AGGs for FSI^- (744 cm^{-1}, one $TFSI^-$ binding with one Li^+ and one FSI^- binding with two or more Li^+) and AGGs for $TFSI^-$ (752 cm^{-1}, one $TFSI^-$ binding with two or more Li^+) [24]. Notably, there is no vibration signal at 736 cm^{-1} corresponding to free $TFSI^-$ anions, indicating that nearly all $TFSI^-$ coordinate with Li^+, verifying the strong coordination ability of $TFSI^-$. Besides, the band at 725 cm^{-1} in LDD and LTDD originates from the C–O-C bending of DOL (Fig. S6 in Supporting information) [34]. The percentages of these ionic speciation were calculated from the peak area and are marked in Fig. 1e. The single-salt-single-solvent electrolyte LD contains 13.7% of free FSI^-, 44.3% of CIPs (FSI^-) and 42.0% AGGs

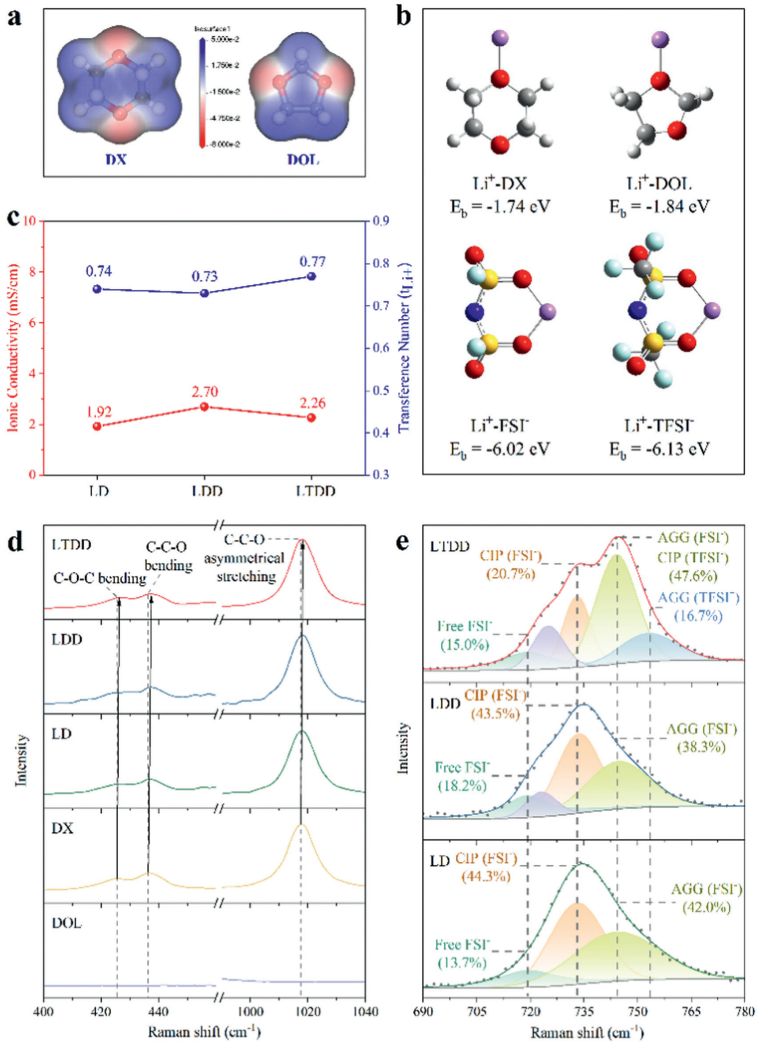

Fig. 1. (a) ESP distributions of DX and DOL. (b) DFT calculation of the binding energy of Li^+-DX, Li^+-DOL, Li^+-FSI^- and Li^+-$TFSI^-$. (c) Ionic conductivity and t_{Li+} of LD, LDD and LTDD. Raman spectra of DOL, DX, LD, LDD and LTDD (d) in the region from 400 cm^{-1} to 1040 cm^{-1} (C–O bending and C–C–O stretching mode of DX) and (e) from 690 cm^{-1} to 780 cm^{-1} (S–N–S symmetric stretching mode of the FSI^- and $TFSI^-$ anions).

(FSI^-), demonstrating that the primary solvation sheath was dominated by anions due to the weakly-solvated characteristic. In LDD, along with the introduction of DOL, the proportion of free FSI^- increases to 18.2%, while the proportions of CIPs (FSI^-) and AGGs (FSI^-) decreases to 43.5% and 38.3% respectively, indicating that DOL displaces partial anions to coordinate with Li^+ and some FSI^- were expelled out of the primary solvation sheath. Fortunately, the proportions of CIPs and AGGs re-increase with the introduction of LiTFSI in LTDD, which contains 15.0% free FSI^-, 20.7% CIPs (FSI^-), 47.6% CIPs ($TFSI^-$) and AGGs (FSI^-), and 16.7% AGGs ($TFSI^-$). Specifically, a higher proportion of free anions corresponds to increased ionic conductivity, while a higher proportion of CIPs and AGGs correlates with increased t_{Li^+} [35]. The observed trend in the percentage of ionic speciation is consistent with the trends in both ionic conductivity and t_{Li^+} for the three investigated electrolytes (Fig. S7 in Supporting information). Such solvation structures were consistent with molecular dynamics (MD) simulations (Fig. S8 in Supporting information). DOL participates in the solvation sheath, resulting in the decrease of the coordination number of anions, which is re-increased by the introduction of $TFSI^-$.

On the basis of the well-formulated WSEs, Gr anode was investigated to validate the impact of solvation structures on interfacial chemistry and electrochemical performance. The cyclic voltammetry (CV) investigations were conducted with the initial cycle presented in Fig. 2a. It can be detected that the investigated electrolytes clearly reveal three pairs of redox peaks between 0.05 V and 0.25 V, indicating the reversible (de)intercalation of Li^+ into Gr anodes. The curves observed in the voltage range of 0.25–1.50 V are indicative of SEI formation, with DOL-reduction peaks appearing at ~1.20 V (coordinated with FSI^-) and ~0.5 V (coordinated with $TFSI^-$) in LDD and LTDD, suggesting the supplementary film-forming effect of DOL (Fig. 2a inset) [28]. The charge/discharge behavior is then studied to detect the reversibility and output capacity (Fig. 2b). Benefiting from the unique solvation structure, the investigated DX-based electrolytes exhibit higher reversible capacities (~360 mAh/g) than carbonate-based electrolyte LB010 (347 mAh/g). Moreover, LTDD reveals the lowest polarization of 30 mV and a high initial coulombic efficiency (CE) of 89.84% owing to the anions-dominant reduction process, demonstrating the synergetic effect of $TFSI^-$ anion and DOL compared to the single addition of DOL. This helps LTDD with rapid ion transport dynamics in electrolyte and electrode, which would result in excellent rate performance. As a validation, the rate capability is further investigated (Figs. 2c and d). It can be observed that all the DX-based electrolytes demonstrate a high reversible capacity of over 357 mAh/g for Gr anode at a low rate of 0.2 C, better than that obtained with

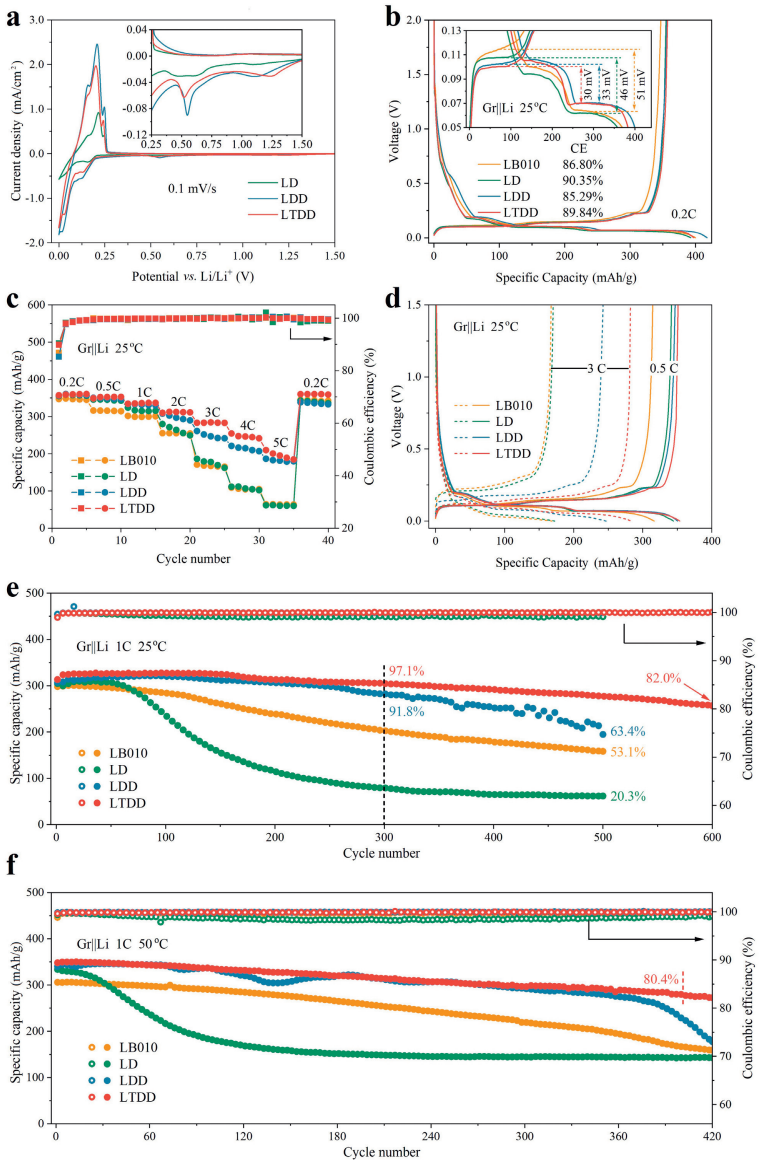

Fig. 2. (a) First-cycle CV curves of Gr||Li cells with various electrolytes. (b) First-cycle charge-discharge curves of Gr||Li cells with various electrolytes and comparison of polarization. (c) Rate performances of Gr||Li cells with various electrolytes at 25 °C. (d) The corresponding charge and discharge curves at specific rates. Long-term cycling performances of Gr||Li cells with various electrolytes at (e) 25 °C and (f) 50 °C.

LB010 electrolyte, indicating the benefits of weakly solvated characteristics. The introduction of DOL enables LDD with acceptable rate performance compared to LD yet inferior to LTDD with two additives of $TFSI^-$ and DOL. Among all the electrolytes, LTDD does exhibit the highest capacity of 210 mAh/g even up to the high rate of 5 C, corresponding to a high capacity retention of 58.3% compared to its capacity at 0.2 C. Upon returning to the rate of 0.2 C, the capacity of LTDD is entirely restored, while other electrolytes experience capacity loss. This demonstrates that the presence of organic species improves the stability of SEI, allowing it to withstand the rapid (de)intercalation of Li^+ under high currents.

Considering the exceptional rate performance of LTDD, the cycling performance is also explored to further unveil the electrochemical stability (Fig. 2e and Fig. S9 in Supporting information). Gr anode with LD electrolyte undergoes rapid capacity decay and only retains 20.3% of its initial capacity after 500 cycles. This might be attributed to the fragile nature of inorganic-rich SEI lacking sufficient organic species, which would result in SEI cracking and increased resistance during cycling. On the contrary, cycling performance of LDD markedly improve with a capacity retention of 91.8% after 300 cycles benefiting from a more stable SEI, which is superior to LB010. Nevertheless, as the cycling continues, the resistance progressively increases and Li^+ transfer kinetics in SEI of LDD becomes obstructed, resulting in significant capacity fluctuations after 400 cycles and a decrease in capacity retention to 63.4% after 500 cycles. Surprisingly, LTDD demonstrates magnificent cycling performance with high capacity retentions of 97.1% after 300 cycles and 82.0% after 600 cycles, obviously outperforming other electrolytes. The achieved cycling performance is significantly improved compared with previous work of weakly solvated ether-based electrolytes for Gr anode [24,28]. The rate performance and cycling stability at room temperature well indicates the advantages of LTDD with the two additives of $TFSI^-$ and DOL. In addition, the charge/discharge performance at elevated temperatures were also evaluated in order to further investigate the stability of the formulated electrolytes. All electrolytes display increased reversible capacity when operated at a high temperature of 50 °C due to the accelerated dynamics of ion transport (Fig. S10 in Sup-

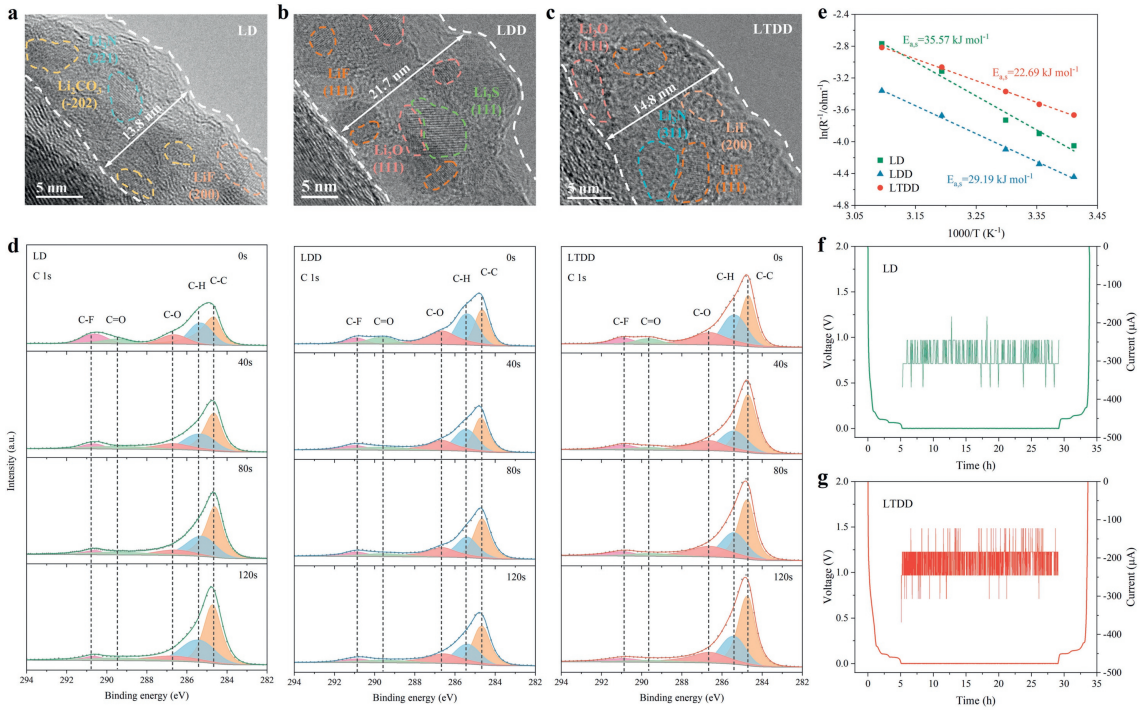

Fig. 3. High-resolution TEM images of SEI formed in (a) LD, (b) LDD and (c) LTDD. (d) The C 1s XPS spectra of SEI formed in various electrolytes. (e) Activation energy of Li^+ transporting across the SEI formed in various electrolytes. (f, g) GC–CA curves of Gr||Li cells with LDD and LTDD.

porting information). As excepted, LTDD performs best at elevated with a high reversible capacity of 363 mAh/g at 0.2 C. The cycling stability examines the quality of SEI layer, where the organic components of SEI are inherently unstable and prone to dissolution in the electrolyte at high temperature [36,37]. It can be detected from Fig. 2f that the LTDD still demonstrates superior performance with a high capacity retention of 80.4% after 400 cycles, while LDD experiences a dramatic decline in capacity after 380 cycles. In contrast, SEI formed in LD electrolyte lacks organic components, making it susceptible to the damage caused by Gr expansion during long cycles, leading to rapid capacity degradation. While LDD introduces some organic components into the SEI, it comes at the expense of compromising its rigidity and conductivity. As a result, the SEI thickens over cycling, leading to increased resistance and decreased capacity as the battery undergoes repeated charge and discharge cycles. The exceptional electrochemical capabilities of LTDD are attributed to the combination of high mechanical strength, compact structure and ionic conductivity of SEI, which is enriched with abundant inorganic species. The presence of organic species in the SEI imparts flexibility, enabling it to withstand the expansion of Gr anodes and thus contributing significantly to the excellent performance of LTDD electrolyte.

As previously mentioned, the electrochemical performance of Gr anodes is greatly influenced by the properties of SEI. Therefore, interfacial characterizations were conducted to analyze the SEI derived in different electrolytes. Transmission electron microscope (TEM) measurements were conducted to elucidate the specific structure of SEI. The SEI in LD and LTDD show similar thickness of 13.8 nm and 14.8 nm, while the introduction of organic components results in the thickening of SEI in LDD to 21.7 nm (Figs. 3a-c). The SEI in all three electrolytes contain abundant inorganic species like LiF, Li_2O and Li_3N, which is favorable for the fast transport of Li^+ crossing the SEI. Nevertheless, unlike the laminar structure of SEI in LD, the SEI in LDD and LTDD present a mosaic-type structure with large contents of inorganic components compactly embedded within the organic layer, which is advantageous for maintaining the stability of SEI in long-term cycling. The discrepancy in the thickness and chemical components of the SEI formed in the three electrolytes was further assessed by X-ray photoelectron spectroscopy (XPS) characterizations with Ar^+ sputtering. The atomic ratios of C, F, O, S and N elements on Gr anodes cycled in LD and LTDD exhibit a consistent trend along with the etching depth changing (Fig. S11 in Supporting information). After sputtering for 40 s, the proportion of C increases rapidly while the ratios of other elements show a declining trend. This indicates that the SEI films in LD and LTDD are extremely thin and the etching quickly reaches the Gr layer. In contrast, the proportion of each element remains relatively stable after sputtering for 40 s in LDD, suggesting that the SEI film is sufficiently thick and the etching does not reach the Gr layer, which is consistent with the TEM results. The C 1s spectra confirm these etching results, showing that the intensity of the peak corresponding to C–C in Gr layers (284.7 eV) rapidly increases as the etching progresses in LD and LTDD, while it changes slightly in LDD (Fig. 3d). Besides, stronger signals of C–O (286.6 eV) and C=O (289.5 eV) are detected in LDD and LTDD, indicating more organic species within SEI film, which corresponds well to the O–C=O species (532.8 eV) in O 1s spectra (Fig. S12 in Supporting information). Strong peaks of LiF (685.7 eV) can be detected from F 1s spectra in all three electrolytes, demonstrating the presence of abundant inorganic species formed from decomposition of anions, facilitating high conductivity of SEI (Fig. S13 in Supporting information). Other inorganic species like Li_2O (529.3 eV), $LiSO_x$ (167.8 eV), Li sulfides (161 ~165 eV) and Li_3N (399.4 eV) are also obviously observed in O 1s spectra, S 2p spectra and N 1s spectra (Fig. S12, S14 and S15 in Supporting information). Additionally, the signals of -SO_2- (170.7 eV) and N-S (400.7 eV) provide further evidence for the involvement of anions in the decomposition process to form SEI.

Temperature-dependent electrochemical impedance spectroscopy (EIS) measurements were further conducted to investigate the kinetics of various interfacial processes (Fig. S16 in Supporting information). The semi-circles presented in the Nyquist plots rep-

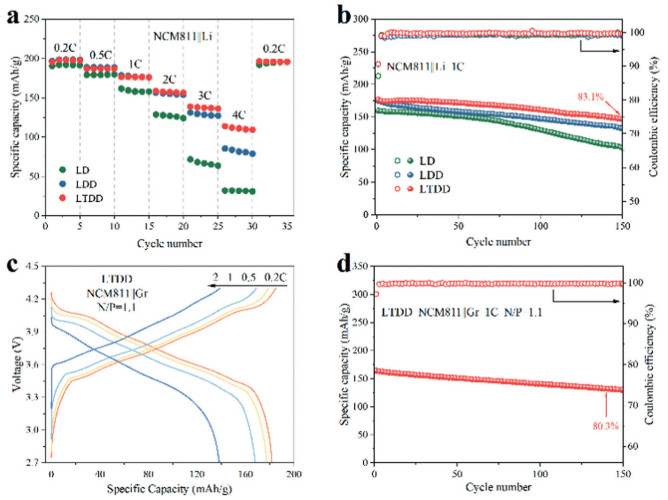

Fig. 4. (a) Rate performances of NCM811||Li cells with various electrolytes. (b) Long-term cycling performances of NCM811||Li cells with various electrolytes. (c) The charge/discharge curves of NCM811||Gr full cells with LTDD electrolyte at various rates. (d) Long-term cycling performance of NCM811||Gr cells with LTDD electrolyte.

resent the combination of Li^+ transporting through SEI (R_{SEI}) and the desolvation step of Li^+. SEI formed in LTDD shows the lowest resistance attributing to the rapid desolvation process and fast Li^+ migration through SEI layer. The former is attributed to the weak coordination between Li^+-DX and the latter is ascribed to accelerated Li^+ migration resulting from dense inorganic composition. According to the Arrhenius law, the logarithm of the impedance is linearly related to the reciprocal of temperature [38]. Based on this, the activation energy (E_a) of combined desolvation process and Li^+ migration process in various electrolytes were calculated and presented in Fig. 3e. LTDD electrolyte shows a low activation energy of 22.69 kJ/mol, indicating that ion conduction is more facile in SEI layer obtained with LTDD electrolyte. Furthermore, the quality of SEI films was evaluated using galvanostatic cycling-chronoamperometry (GC–CA) test with different electrolytes (Figs. 3f and g, Fig. S17 in Supporting information). Gr anode cycled in LTDD exhibits the lowest leakage current, indicating a more stable and uniform SEI film, thereby effectively preventing side effects and facilitating long-term cycling of Gr anodes. These interfacial analysis results demonstrate that the synergistic effect of DOL and $TFSI^-$ contributes to the formation of a thinner and more uniform inorganic-rich SEI film containing sufficient organic species, which is conducive to the fast transport of Li^+ and the maintenance of long cycle stability.

The bisalt DX-based weakly-solvated electrolyte LTDD has shown remarkable efficacy on the Gr anode side, owing to its distinctive solvation structure and the formation of a stable SEI film. To further assess its potential for commercial applications, the electrochemical compatibility with high-voltage NCM811 cathodes is investigated. Linear sweep voltammetry (LSV) measurements reveal that the three DX-based electrolytes all exhibit high oxidation potential exceeding 5 V, implying their excellent adaptability on cathodes (Fig. S18 in Supporting information). Moreover, charge/discharge tests of NCM811 cathodes in these electrolytes were conducted under different cut-off potential at a small rate of 0.2 C (1 C = 200 mAh/g) (Fig. S19 in Supporting information). All DX-based electrolytes can withstand a charging voltage of 4.5 V maintaining a high reversible capacity of ~210 mAh/g, implying their excellent cathodic stability. Considering the practical cycling stability, the voltage range for electrochemical performance tests of NCM811 cathodes was 2.7–4.3 V (Fig. 4a and Fig. S20 in Supporting information). The reversible capacity of NCM811 cathode in LD rapidly deteriorates at high rates, despite that it exhibits a high reversible capacity of 191 mAh/g at the small rate of 0.2 C (1 C is represented as 200 mAh/g). The introduction of DOL substantially improves the rate capability. LTDD outperforms other two electrolytes with a high reversible capacity of 140 mAh/g at 3 C, corresponding to a high capacity retention of 70.8% compared to its capacity at 0.2 C. Moreover, the NCM811 cathode can be stably operated for 150 cycles at the rate of 1 C in LTDD electrolyte, exhibiting a sluggish capacity attenuation and keeps a high retention with 83.1% of initial capacity (Fig. 4b and Fig. S21 in Supporting information). Benefiting from the compatibility of LTDD with Gr anode and NCM811 cathode, full cells were therefore assembled to amplify the avail of LTDD. According to the electrochemical performance of half cells, the full cell was designed with a N/P ratio of 1.1 and voltage range of 2.7–4.3 V. It can be detected from the charge/discharge curves that the full cell displays a reversible capacity of 182 mAh/g at the small rate of 0.2 C, and keeps 130 mAh/g when increasing the rate to 2 C (Fig. 4c and Fig. S22 in Supporting information). Moreover, the full cells exhibit a remarkable stability for 150 cycles and obtain a capacity retention of 80.3% after 140 cycles, which highlights the exceptional practicability of as-formulated LTDD electrolyte (Fig. 4d and Fig. S23 in Supporting information).

In conclusion, a weakly-solvated bisalt ether-based electrolyte, LTDD, has been well formulated to satisfy both the rapid desolvation process and desired SEI with facile ions movement and excellent stability. On the basis of the anions-dominated solvation sheath, the incorporation of the film-forming additive DOL, which participates in the solvation structure and decomposes into the SEI, contributes to a certain content of organic species for maintaining the stability of SEI. Thanks to the optimized SEI film and solvation structure, the Gr anode exhibits outstanding rate performance (210 mAh/g at 5 C) and remarkable cycling stability, retaining 82% of its capacity after 600 cycles at room temperature (25 °C). Furthermore, the Gr anodes maintain exceptional cycling stability for over 400 cycles at a high temperature of 50 °C. Moreover, LTDD demonstrates impressive compatibility with high-voltage NCM811 cathodes, showcasing excellent rate capability of 140 mAh/g at 3 C. Additionally, the NCM811||Gr full cell with LTDD electrolyte delivers a high reversible capacity of 170 mAh/g and maintains stable cycling for over 150 cycles. This study highlights the effective modification of weakly-solvated electrolytes to optimize the performance of graphite anodes and graphite-based lithium-ion batteries.

Declaration of competing interest

There are no conflicts of interest to declare.

Acknowledgments

We gratefully acknowledge the support from the National Key Research and Development Program of China (No. 2022YFB2402200), National Natural Science Foundation of China (No. 22109028), Natural Science Foundation of Shanghai (No. 22ZR1404400), Chenguang Program sponsored by Shanghai Education Development Foundation and Shanghai Municipal Education Commission (No. 19CG01).

Supplementary materials

Supplementary material associated with this article can be found, in the online version, at doi:10.1016/j.cclet.2023.109146.

References

[1] L.D. Xing, X.W. Zheng, M. Schroeder, et al., Acc. Chem. Res. 51 (2018) 282–289.
[2] J.L. Gai, J.R. Yang, W. Yang, et al., Chin. Phys. Lett. 40 (2023) 086101.
[3] D. Zhang, L. Li, W.Z. Zhang, et al., Chin. Chem. Lett. 34 (2023) 107122.
[4] S.C. Zhang, S.Y. Li, Y.Y. Lu, eScience 1 (2021) 163–177.
[5] J.M. Yuan, N. Qin, Y.Y. Lu, et al., Chin. Chem. Lett. 33 (2022) 3889–3893.
[6] H.R. Cheng, Q.J. Sun, L.L. Li, et al., ACS Energy Lett. 7 (2022) 490–513.
[7] J.D. Huang, Y.H. Zhu, Y. Feng, et al., Acta Phys. Chim. Sin. 38 (2022) 2208008.
[8] Y.X. Zou, F.Y. Cheng, Y. Lu, et al., Small 19 (2023) 2203394.
[9] T.R. Jow, S.A. Delp, J.L. Allen, et al., J. Electrochem. Soc. 165 (2018) A361–A367.
[10] Y. Yang, Z. Fang, Y. Yin, et al., Angew. Chem. Int. Ed. 61 (2022) e202208345.
[11] M. Li, C.S. Wang, Z.W. Cheng, et al., Chem. Rev. 120 (2020) 6783–6819.
[12] Y. Yang, P.L. Li, N. Wang, et al., Chem. Commun. 56 (2020) 9640–9643.
[13] Y.X. Yao, J. Wan, N.Y. Liang, et al., J. Am. Chem. Soc. 145 (2023) 8001–8006.
[14] X.J. Xu, X.Y. Yue, Y.M. Chen, et al., Angew. Chem. Int. Ed. 62 (2023) e202306963.
[15] S.H. Jiao, X.D. Ren, R.G. Cao, et al., Nat. Energy 3 (2018) 739–746.
[16] W. Wang, J.L. Zhang, Q. Yang, et al., ACS Appl. Mater. Interfaces 12 (2020) 22901–22909.
[17] X. Cao, H. Jia, W. Xu, et al., J. Electrochem. Soc. 168 (2021) 010522.
[18] L.L. Jiang, C. Yan, Y.X. Yao, et al., Angew. Chem. Int. Ed. 60 (2021) 3402–3406.
[19] G. Song, Z.L. Yi, F.Y. Su, et al., ACS Energy Lett. 8 (2023) 1336–1343.
[20] Y.B. Mo, G.P. Liu, Y. Yin, et al., Adv. Energy Mater. 13 (2023) 2301285.
[21] D.J. Yoo, Q. Liu, O. Cohen, et al., Adv. Energy Mater. 13 (2023) 202204182.
[22] J.J. Xu, J.X. Zhang, T.P. Pollard, et al., Nature 614 (2023) 694–700.
[23] T.D. Pham, A. Bin Faheem, J. Kim, et al., Small 18 (2022) 2107492.
[24] Y.X. Yao, X. Chen, C. Yan, et al., Angew. Chem. Int. Ed. 60 (2021) 4090–4097.
[25] S. Lei, Z.Q. Zeng, M.C. Liu, et al., Nano Energy 98 (2022) 107265.
[26] T.D. Pham, A. Bin Faheem, H.D. Nguyen, et al., J. Mater. Chem. A 10 (2022) 12035–12046.
[27] Y.Q. Liao, M.Y. Zhou, L.X. Yuan, et al., Adv. Energy Mater. 13 (2023) 202301477.
[28] D.W. Xia, E.P. Kamphaus, A.Y. Hu, et al., ACS Energy Lett. 8 (2023) 1379–1389.
[29] H.Z. Jiang, C. Yang, M. Chen, et al., Angew. Chem. Int. Ed. 62 (2023) e202300238.
[30] Q. Zhao, X.T. Liu, S.J. Stalin, et al., Nat. Energy 4 (2019) 365–373.
[31] Q.L. Wang, Z.L. Cui, Q. Zhou, et al., Energy Storage Mater. 25 (2020) 756–763.
[32] K.M. Diederichsen, E.J. McShane, B.D. McCloskey, ACS Energy Lett. 2 (2017) 2563–2575.
[33] Y.X. Chen, A.J. Li, Y. Zhao, et al., Eur. Phys. J. D 74 (2020) 121.
[34] V. Mohacek-Grosev, K. Furic, H. Ivankovic, Vib. Spectrosc. 64 (2013) 101–107.
[35] Y. Zhao, T.H. Zhou, T. Ashirov, et al., Nat. Commun. 13 (2022) 2575.
[36] M. Koltypin, D. Aurbach, L. Nazar, et al., J. Power Sources 174 (2007) 1241–1250.
[37] A. Tomaszewska, Z.Y. Chu, X.N. Feng, et al., eTransportation 1 (2019) 100011.
[38] Y.S. Yang, Y.F. Chen, L.L. Tan, et al., Angew. Chem. Int. Ed. 61 (2022) e202209619.